



<http://www.diva-portal.org>

Postprint

This is the accepted version of a paper published in *Proceedings / IEEE International Conference on Robotics and Automation*. This paper has been peer-reviewed but does not include the final publisher proof-corrections or journal pagination.

Citation for the original published paper (version of record):

Nikou, A. (2015)

Mechanical design, modelling and control of a novel aerial manipulator

Proceedings / IEEE International Conference on Robotics and Automation

Access to the published version may require subscription.

N.B. When citing this work, cite the original published paper.

Permanent link to this version:

<http://urn.kb.se/resolve?urn=urn:nbn:se:kth:diva-264983>

Mechanical Design, Modelling and Control of a Novel Aerial Manipulator

Alexandros Nikou, Georgios C. Gavridis and Kostas J. Kyriakopoulos

Abstract—In this paper a novel aerial manipulation system is proposed. The mechanical structure of the system, the number of thrusters and their geometry will be derived from technical optimization problems. The aforementioned problems are defined by taking into consideration the desired actuation forces and torques applied to the end-effector of the system. The framework of the proposed system is designed in a CAD Package in order to evaluate the system parameter values. Following this, the kinematic and dynamic models are developed and an adaptive backstepping controller is designed aiming to control the exact position and orientation of the end-effector in the Cartesian space. Finally, the performance of the system is demonstrated through a simulation study, where a manipulation task scenario is investigated.

I. INTRODUCTION

Aerial manipulation is a new scientific field which has been gaining significant research attention and a wide variety of structures have been proposed in the last years. These manipulation systems possess several features which have lately brought them in the spotlight, with their objective mainly oriented towards performing effectively complex manipulating tasks in unstructured and dynamic environments. Having them include active manipulation as a major functionality, would vastly broaden the applications of these systems, as they move from mere passive observation and sensing to interaction with the environment. Therefore, new scientifically applicable horizons will be introduced related to cooperative manipulation, surveillance, industrial inspections, inspection and maintenance of aerial power lines, assisting people in rescue operations and constructing in inaccessible sites by repairing and assembling. Naturally, both designing and controlling aerial manipulators could be considered as nontrivial engineering challenges.

The first theoretical and experimental results on aerial robots interacting with the environment were developed in [1], [2] using a ducted-fan prototype UAV within the framework of AIRobots project. The design of a quadrotor capable of applying force to a wall maintaining flight stability was performed in [3]. In [4] experimental results with a small helicopter with grasping capabilities were derived, along with the stability proofs while grasping. Several grippers that allow quadrotors to grasp, pick up and transport payloads were introduced in [5]. An implementation of indoor gripping using a low-cost quadrotor has been introduced in [6]. The

authors in [7] addressed the problem of controlling multiple quadrotor robots that cooperatively grasp and transport a payload in three dimensions. Another significant work with cooperative quadrotors throwing and catching a ball with a net was performed in [8].

A dexterous holonomic hex-rotor platform equipped with a six DoF end-effector that can resist any applied wrench was proposed in [9]. A system for aerial manipulation, composed of a helicopter platform and a fully actuated seven DoF redundant robotic arm, has been introduced in [10]. Another hex-rotor manipulator that consists of three pair of propellers with a two-link manipulator aiming to trajectory tracking control was studied in [11].

More recently, significant experiments using commercial quadrotors equipped with external robotic arms have been conducted in [12]–[14].

In this work, a completely novel aerial manipulator is introduced. This could be considered as a small autonomous aerial robot that interacts with the environment via an end-effector by applying desired forces and torques in a 6 DoF task space. The proposed system provides mechanical design flexibility achieved through technical optimization problems. The structural geometric distribution is the outcome of the aforementioned problems with the main goals being oriented towards low body volume, controllability of the system, avoidance of possible aerodynamic interactions and efficiency in performing desired manipulation tasks in dynamic environments. The system is fully integrated as it is not a commercial aerial robot equipped with an external robotic arm, as many of the aerial manipulators mentioned above. The optimal number of thrusters, their positions/orientations and the optimal position of the end-effector on the body structure are defined with respect to the modelling design limitations. Taking all the above into account, the remaining challenge is to actually construct this novel aerial robot.

The rest of paper is organized as follows. In Section II a functional description of the robot and the mechanical design analysis is discussed. A mathematical model that captures the proposed system dynamics and govern the behaviour of the system is derived in Section III. Based on this highly nonlinear model, an adaptive backstepping control law is designed in Section IV. In Section V, simulation results are presented in order to study the performance of the system. Finally, the main conclusions are discussed in Section VI.

II. MECHANICAL DESIGN

The overall description of the Aerial Manipulator was based on the idea of designing an aerial robot composed

Alexandros Nikou, Georgios C. Gavridis and Kostas J. Kyriakopoulos are with the Control Systems Lab, Department of Mechanical Engineering, National Technical University of Athens, 9 Heroon Polytechniou Street, Zografou 15780, Greece. Email: {mcp12214, mc08042, kkyria}@mail.ntua.gr

of a set number n of similar thrusters and an end-effector, in order to interact with objects in the environment. The exact geometry of the structure will be the result of the analysis of this section.

A. Principles of the Problem

Initially, we define the Body-Fixed frame and the End-Effector frame as $F_B = \{\hat{x}_B, \hat{y}_B, \hat{z}_B\}$, $F_E = \{\hat{x}_E, \hat{y}_E, \hat{z}_E\}$. These frames are attached to the rigid body of the aerial manipulator as in Fig. 1. The vectors $r_i, r_e \in \mathbb{R}^3$ denote the position of each thruster and the position of the end-effector respectively with reference to the Body-Fixed frame. The thruster orientations are given by the unit vectors $\hat{F}_i \in \mathbb{R}^3$, $i = 1, \dots, n$, the thrust forces are defined as λ_i and the propulsion vectors are given by $\lambda_i \hat{F}_i$. At this point, it is assumed that the total system is considered to be a rigid body and, without loss of generality, the End-Effector frame and the Body frame have the same orientation. Thus, the actuation force applied to the end-effector is $F_{act}|_B = F_{act}|_E \in \mathbb{R}^3$, where $|_B, |_E$ denote the expressions to the frames F_B, F_E respectively. The corresponding actuation torque is obtained via the formula $T_{act}|_B = T_{act}|_E + r_e \times f_e$ where $T_{act}|_E = r \times f_e$ is the torque produced by the end-effector. The terms r, f_e denote the displacement vector (length of the lever arm) and the vector force that tends to rotate a gripped object from the end-effector.

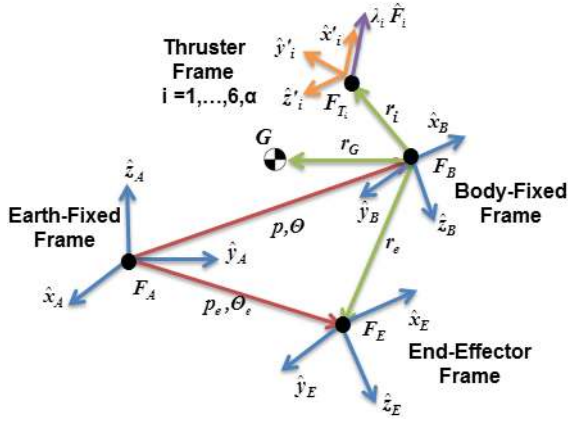


Fig. 1: Aerial Manipulator Frame Configuration System

B. Forces and Torques

The forces transmitted essentially through the end-effector are written as

$$\sum_{i=1}^n (\lambda_i \hat{F}_i) + W = F_{act}|_B \quad (1)$$

where $W \in \mathbb{R}^3$ is the vector that corresponds to the total weight of the system. By separating the weight as $w_s = W - n w$, where $w \in \mathbb{R}^3$ is the weight of each thruster, (1) is modified as

$$F \lambda + n w + w_s = F_{act}|_B \quad (2)$$

where $\lambda = [\lambda_1 \dots \lambda_n]^T \in \mathbb{R}^n$ and $F = [\hat{F}_1 \dots \hat{F}_n]^T \in \mathbb{R}^{3 \times n}$.

Similarly, the torque from each thruster is $T_i = r_i \times (\lambda_i \hat{F}_i) = \lambda_i S(r_i) \hat{F}_i$. The well-known skew-symmetric matrix $S(\cdot) \in \mathbb{R}^{3 \times 3}$ is defined as $a \times b = S(a) b$ for the cross-product \times and any vectors $a, b \in \mathbb{R}^3$. The torque due to the weight is calculated as

$$T_W = r_G \times W = \sum_{i=1}^n r_i \times w + r_s \times w_s = \sum_{i=1}^n S(r_i) w + S(r_s) w_s$$

where r_G is the centre of gravity of the system and r_s is the centre of gravity of the system, when omitting the mass of each thruster (m_{thr}). The reaction torque of each thruster is $\tau_i = \mu (\lambda \hat{F}_i)$ where μ is a coefficient that represents the relationship between the thrust force and the reaction torque [15]. Therefore, by combining all torques the following equation holds

$$\sum_{i=1}^n \left\{ \lambda_i S(r_i) \hat{F}_i \right\} + \mu \sum_{i=1}^n (\lambda_i \hat{F}_i) + \sum_{i=1}^n S(r_i) w + S(r_s) w_s = T_{act}|_B \quad (3)$$

Using the matrices

$$r = [r_1 \dots r_n]^T \in \mathbb{R}^{3 \times n}, \bar{F} = F_{act}|_B - n w - w_s \quad (4)$$

$$E(r, F) = [S(r_1) \hat{F}_1 \dots S(r_n) \hat{F}_n] \in \mathbb{R}^{3 \times n} \quad (5)$$

in (2),(3) we get

$$\begin{cases} F \lambda = \bar{F} \\ E \lambda = T_{act}|_B - \mu \bar{F} - \sum_{i=1}^n S(r_i) w - S(r_s) w_s \end{cases} \quad (6)$$

By defining the matrix $D(r, F) = \begin{bmatrix} F \\ E(r, F) \end{bmatrix} \in \mathbb{R}^{6 \times n}$, from the system (6) it is implied that

$$D(r, F) \lambda = W_R \quad (7)$$

where the augmented wrench vector $W_R \in \mathbb{R}^6$ is given by

$$W_R = \begin{bmatrix} \bar{F} \\ T_{act}|_B - \mu \bar{F} - \sum_{i=1}^n S(r_i) w - S(r_s) w_s \end{bmatrix} \quad (8)$$

C. Negative Thrust Forces

It is clear that when solving (7), the vector that corresponds to the thrust force λ can obtain any value in \mathbb{R}^6 . However, the thrusters are optimally designed to produce thrust force towards a specific direction, which we set to correspond to the positive values of λ_i . In order to alleviate the problem of negative λ_i , a conservative solution is adopted in this analysis, which is based on the idea of introducing one additional thruster. Thus, (7) is rewritten as

$$\sum_{i=1}^n \lambda_i t_i = W_R \quad (9)$$

where

$$D(r, F) = [t_1 \ t_2 \ \dots \ t_n] \text{ and } t_i = \begin{bmatrix} \hat{F}_i \\ S(r_i) \hat{F}_i \end{bmatrix} \in \mathbb{R}^6 \quad (10)$$

for all $i = 1, \dots, n$. The vector

$$t_a = - \sum_{i=1}^n t_i = \begin{bmatrix} - \sum_{i=1}^n \hat{F}_i \\ - \sum_{i=1}^n \{S(r_i) \hat{F}_i\} \end{bmatrix} = \begin{bmatrix} \hat{F}_a \\ S(r_a) \hat{F}_a \end{bmatrix} \quad (11)$$

that corresponds to the additional thruster is introduced. Using (11), the position vector r_a and the direction \hat{F}_a of the new thruster should satisfy the equations $\hat{F}_a = - \sum_{i=1}^n \hat{F}_i$, $S(\hat{F}_a) r_a = - \sum_{i=1}^n \{S(\hat{F}_i) r_i\}$.

If we assume that (7) results in some negative thrust forces, then the set $\sigma_N = \{k : \lambda_k < 0, k = 1, \dots, 6\}$ denotes the indexes for every negative thrust force and $\sigma_P = \{1, 2, 3, 4, 5, 6\} - \sigma_N$ the corresponding set of positive thrust forces. Observing that $\lambda_k < 0 \Leftrightarrow (-\lambda_k) > 0, \forall k \in \sigma_N$, (9) can be separated in

$$\begin{aligned} \sum_{i \in \sigma_P} \lambda_i t_i + \sum_{k \in \sigma_N} \lambda_k t_k &= W_R \\ \Leftrightarrow \sum_{i \in \sigma_P} \lambda_i t_i + \sum_{k \in \sigma_N} (-\lambda_k) (-t_k) &= W_R \end{aligned} \quad (12)$$

Now, from (11) the following can be exported

$$t_a = - \sum_{i=1}^n t_i = - \sum_{i \in \sigma_P} t_i - \sum_{j \in \sigma_N} t_j \quad (13)$$

It is obvious that

$$- \sum_{j \in \sigma_N} t_j = -t_k - \sum_{\substack{j \in \sigma_N \\ j \neq k}} t_j, \forall k \in \sigma_N \quad (14)$$

Combining (13), (14) we obtain

$$-t_k = t_a + \sum_{i \in \sigma_P} t_i + \sum_{\substack{j \in \sigma_N \\ j \neq k}} t_j, \forall k \in \sigma_N \quad (15)$$

By substituting (15) into (12) we have

$$\sum_{i \in \sigma_P} \lambda_i t_i + \sum_{k \in \sigma_N} (-\lambda_k) \left[t_a + \sum_{i \in \sigma_P} t_i + \sum_{\substack{j \in \sigma_N \\ j \neq k}} t_j \right] = W_R$$

Defining

$$\Delta = \sum_{k \in \sigma_N} (-\lambda_k) > 0, E_k = \sum_{\substack{j \in \sigma_N \\ j \neq k}} (-\lambda_j) > 0 \quad (16)$$

and rearranging the terms we result in

$$\sum_{i \in \sigma_P} (\lambda_i + \Delta) t_i + \sum_{k \in \sigma_N} E_k t_k + \Delta t_a = W_R \quad (17)$$

From (17) the thruster redistribution among all thrusters after adding the new thruster is provided. It has been proven that the issue of negative thrust forces can be alleviated with adding one extra thruster. This equation can be better analysed in Fig. 2 in which the thrust redistribution algorithm is depicted. The variables $\lambda', \lambda'_i, \lambda'_k$ denote the initial thrust forces and the other variables the thrust force after the

redistribution, plus the additional thrust force λ_a . Thus, the six thrust forces (not necessary all positive) are equivalent to seven thrust forces, all positive with redistributed thrust forces as in (17). By using the additional thruster, (4), (8) are reformed into

$$\bar{F} = F_{act}|_B - (n+1) w - w_s \quad (18)$$

$$W_R = \begin{bmatrix} \bar{F} \\ T_{act}|_B - \mu \bar{F} - \sum_{i=1}^{n+1} S(r_i) w - S(r_s) w_s \end{bmatrix} \quad (19)$$

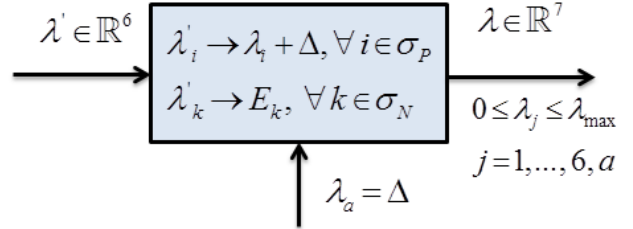


Fig. 2: Thrust Force Equivalence

D. Aerodynamic Interaction

At this point, the aerodynamic interaction between the operation thrusters is investigated. The aerodynamic effects produced by each thruster, are based on experiments that took place in Control Systems Lab NTUA on a $8 \times 4.7SF$ APC propeller accompanied with the Neu Motor NEU 1902/2Y - 2035 motor, which produces at 17550 rpm, a $\lambda_{\max} = 28N$ thrust force. The surface, corresponding to every thruster, that approximates these effects is described by a third order equation in (SI). By expressing this equation in the thruster frame $F_{T_i} = \{\hat{x}'_i, \hat{y}'_i, \hat{z}'_i\}, i = 1, \dots, 6, a$ we get

$$-0.06 \leq x'_i \leq 0.91 \quad (20)$$

$(y'_i)^2 + (z'_i)^2 \leq [-1.1(x'_i)^3 + 1.56(x'_i)^2 - 0.3(x'_i) + 0.11]^2$
Hence, the aerodynamic effects of the air flow throughout the rotor are extended from $x = -0.06m$ to $x = 0.91m$. The x axis shows the length of the aerodynamic effect of the exit flow. In order to understand this, one should consider the rotor/blade to be positioned at $x = 0$. On the other hand, y axis shows the distance of the effect measured from the rotation axis of the blade, where at position $(x = 0, y = 0.102m)$ (SI) is the blade radius in approximation (because of the existence of an offset).

An arbitrary point $p = [x \ y \ z]^T$ expressed in F_B and the corresponding $p'_i = [x'_i \ y'_i \ z'_i]^T$ expressed in F_{T_i} , can be linked together by the equation $p = \{TR_{F_B}^{F_{T_i}}(r_i, \hat{F}_i)\} p'_i$, where $TR_{F_B}^{F_{T_i}}(r_i, \hat{F}_i)$ is the appropriate homogeneous frame transformation corresponding to the translation and orientation vectors (r_i, \hat{F}_i) . By combining the previous coordinates transformation equation with the constraints (20), a set of constraints that can be described in matrix form as $G(r_i, \hat{F}_i, p) \leq 0$, is produced. The distance between two such volumes i, j can be defined and evaluated via the optimization problem (P_1) of Table I.

E. Design Problem

Given a particular structure defined by the matrices (r, F) , for a set of required actuation forces and torques $(F_{act}|_E, T_{act}|_E)$ it is necessary to find the associate levels of the thrust forces λ_i . Since $W_R \in \mathbb{R}^6$, in order for (7) to have a solution for $\lambda \in \mathbb{R}^n$, the conditions $\{\text{rank}(D) = 6, n \geq 6\}$ are required. The rank condition is adequate from a strict mathematical perspective but from a practical point of view, as (7) leads to the thrust forces values $\lambda \in \mathbb{R}^n$, the sought solutions should not be very sensitive to small deviations. This is partially achieved by using the condition number $\kappa(D) = \sigma_{\max}(D)/\sigma_{\min}(D)$ where $\sigma(D) = \sqrt{\text{eig}(D^T D)}$ are the singular values of the matrix D , $\text{eig}(\cdot)$ denotes the eigenvalues of a matrix and $\sigma_{\max}(D), \sigma_{\min}(D)$ are the maximum and minimum singular values of the matrix D respectively. Thus, a low condition number $\kappa(D) \geq 1$ is required [16]. Although the condition number is bounded to take feasible values (not equal to zero/infinity) when $\sigma(D) \rightarrow 0$, the matrix $D(r, F)$ might be ill-conditioned i.e. $\det(D(r, F)) \rightarrow 0$. Thus, $\sigma(D) \geq \epsilon_1 > 0$. Furthermore, to avoid the fan interaction an other constraint is introduced as $d_{ij}(r_i, \hat{F}_i, r_j, \hat{F}_j) \geq \epsilon_2 > 0, \forall i, j = 1, 2, \dots, n, \alpha$. Note that, similarly to (P_1) , the position r_e should be introduced to the design problem as the intersection avoidance between a sphere (with radius R_e) that encloses the end-effector, and the thrusters. This sphere, when expressed in the End-Effector frame F_E , is given by $(x'_e)^2 + (y'_e)^2 + (z'_e)^2 \leq R_e^2$. Therefore, the constraint associated with the end-effector is $d_{ei}(r_e, r_i) \geq R_e > 0, \forall i = 1, 2, \dots, n, \alpha$. An optimization is also required to minimize the volume of the system, by using the norm $J(r) = \|r\|_2$. Taking all the above into consideration, the design problem is essentially recast to the optimization problem (P_2) from Table I. The optimization parameters are chosen as $K = 5, \epsilon_1 = 10^{-3}, \epsilon_2 = 10^{-2} m, R_e = 10^{-2} m$.

(P_1)	$d_{ij}(r_i, \hat{F}_i, r_j, \hat{F}_j) = \min_{p_i, p_j} \ p_i - p_j\ $ $\text{s.t. } G(r_i, \hat{F}_i, p_i) \leq 0$ $G(r_j, \hat{F}_j, p_j) \leq 0$
(P_2)	$\min_{r, r_e, \hat{F}} J(r)$ $\text{s.t. } \sigma(D) \geq \epsilon_1$ $d_{ij} \geq \epsilon_2, \forall i, j = 1, 2, \dots, n, \alpha$ $d_{ei} \geq R_e, \forall i = 1, 2, \dots, n, \alpha$ $\hat{F}_a = - \sum_{i=1}^n \hat{F}_i$ $S(\hat{F}_a) r_a = - \sum_{i=1}^n S(\hat{F}_i) r_i$ $1 \leq \kappa(D) \leq K$

TABLE I
OPTIMIZATION PROBLEMS

F. Solving the Optimization Problem

It should be noted that when solving the optimization problem (P_2) , each time the inner problem (P_1) should be solved. There are 45 decision variables of the optimization

problem, which correspond to the seven position vectors (r_i) of the thrusters, the position vector (r_e) of the end-effector and the direction vectors (\hat{F}_i) of the seven thrusters. This issue, entails the necessity of solving 28 optimization problems for each evaluation attempt of the outer problem (P_2) .

The inner problem, that refers to the avoidance of the fan interaction, is smooth but in terms of the outer problem (P_2) is nonsmooth and nonlinear. The objective function and the constraints of the problem (P_1) are continuous and this problem, according to the inputs, has one and only one global minimum. Using the appropriate rotation and transformation matrices, the (P_1) was solved by the active-set strategy [17],[18]. On the other hand, the design problem (P_2) has nonsmooth, discontinuous and nonlinear inequality constraints, but smooth objective function. Consequently, a non-gradient-based methodology that searches disjoint feasible regions, is utilized. For the pre-search of the design space, a Latin Hypercube (LHS) [19] was chosen, in order to ensure that the points are distributed throughout the search space. The Latin Hypercube sampling is known to provide better coverage than the simple random sampling [20]. Following this, a Generalized Pattern Search (GPS) direct search algorithm [21],[22] was used.

The thrust force (λ) and the momentum (Q) can be calculated from [23],[24] as

$$\begin{cases} Q = \pi \rho C_Q R^5 \Omega^2 \\ \lambda = \pi \rho C_\lambda R^4 \Omega^2 \end{cases} \Leftrightarrow Q = \frac{C_Q}{C_\lambda} R \lambda \quad (21)$$

where the term $\frac{C_Q}{C_\lambda} R$ corresponds to the coefficient μ , R is the radius of the rotor and ρ, Ω denote the air density and the rotational speed of the rotor respectively. Applying a combination of the Blade Element Theory [24] and the Momentum Theory [15], using the modified versions proposed in [23] and invoking the experimental results extracted by our lab on the APC propeller, it was calculated that $C_\lambda = 0.008, C_Q = 0.0095, \mu = 0.1473, R = 0.124m$. By solving the optimization problems, with the results depicted in Table II, the matrix $D(r, F)$ is full rank and using (7), the thrust forces can be calculated as $\lambda = D^{-1} W_R$. All the constraints were satisfied and a low volume body structure with condition number $\kappa(D) = 3.36$ resulted. The wrench vector W_R can be determined by substituting the desired actuation forces/torques $(F_{act}|_E, T_{act}|_E)$ in (19). The maximum thrust force and torque which can be applied from the system are $\lambda_{\max} = 28N$ and $3Nm$ respectively. The values of the components, proposed for the Aerial Manipulator, are the following: the motor and the propeller (0.12kg), the frame (0.66kg), the battery (0.25kg) and the electronic components (0.15kg). The total mass of the proposed system is $m = 1.90kg$. Ultimately, the production of a carefully studied framework (Fig. 3) was achieved by using the 3D CAD Package SolidWorks. Using this Package, the system parameter values of the Table II have been evaluated.

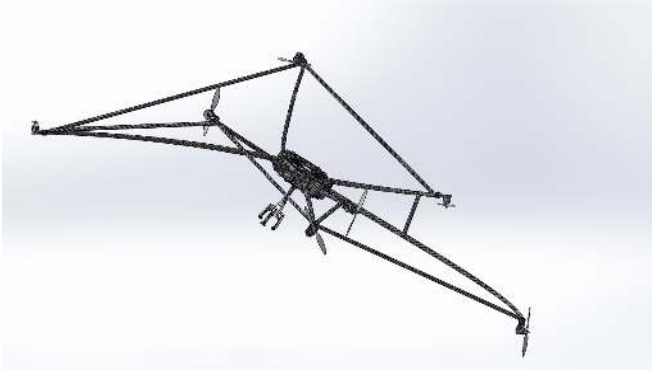


Fig. 3: Aerial Manipulator 3D Caption of the Framework

Param.	Description	Value	Units
m	Total Mass	1.90	kg
m_{thr}	Thruster Mass	0.12	kg
I_G	Moment of Inertia Tensor	$\begin{bmatrix} 0.3488 & 0.0683 & -0.0457 \\ 0.0683 & 0.1588 & 0.0144 \\ -0.0457 & 0.0144 & 0.4081 \end{bmatrix}$	kg m ²
r_G	Centre of Gravity Position	$[0.0737 \ 0.0083 \ -0.0781]^T$	m
r_e	End-Effector Position	$[-0.23 \ 0.015 \ 0.23]^T$	m
r_s	Centre of Grav. from (3)	$[0.1267 \ -0.0052 \ -0.1900]^T$	m
$J(r)$	Total Structure Volume	1.80018	m ³
g	Gravitational Acceleration	9.81	m/s ²
r_i	Thruster Positions	$\begin{aligned} r_1 &= [0.43 \ -0.15 \ -0.44]^T \\ r_2 &= [0.08 \ -0.22 \ -0.14]^T \\ r_3 &= [0.1 \ -0.9 \ -0.2]^T \\ r_4 &= [-0.34 \ 0.25 \ 0.006]^T \\ r_5 &= [0.184 \ 0.359 \ -0.254]^T \\ r_6 &= [-0.22 \ -0.44 \ -0.04]^T \\ r_7 &= [0.51 \ 0.79 \ -0.06]^T \end{aligned}$	m
\hat{F}_i	Thruster Orientations	$\begin{aligned} \hat{F}_1 &= [0.08 \ 0.39 \ 0.92]^T \\ \hat{F}_2 &= [-0.33 \ -0.90 \ 0.29]^T \\ \hat{F}_3 &= [0.13 \ -0.87 \ -0.48]^T \\ \hat{F}_4 &= [0.56 \ 0.08 \ 0.82]^T \\ \hat{F}_5 &= [0.83 \ 0.11 \ -0.55]^T \\ \hat{F}_6 &= [-0.66 \ 0.57 \ -0.49]^T \\ \hat{F}_7 &= [-0.59 \ 0.62 \ -0.51]^T \end{aligned}$	

TABLE II
AERIAL MANIPULATOR PARAMETERS

III. MATHEMATICAL MODEL OF THE AERIAL MANIPULATOR

In this section, the kinematic and dynamic equations of motion in case there are no interaction forces and torques from the environment applied to the end-effector are presented.

A. Kinematic Model

Fig. 1 shows the reference frames defined to derive the kinematic and dynamic model of the proposed system. The Earth-Fixed inertial frame is defined as $F_A = \{\hat{x}_A, \hat{y}_A, \hat{z}_A\}$

and it should be noted that the Body-Fixed frame's origin does not coincide with the centre of gravity G . The position of F_B relative to F_A can be represented by $p = [x \ y \ z]^T \in \mathbb{R}^3$ and the corresponding orientation by the rotation angles $\Theta = [\phi \ \theta \ \psi]^T \in \mathbb{R}^3$. The translational and rotational kinematic equations of the moving rigid body are given (see [25]) in matrix form by

$$\dot{\xi} = \begin{bmatrix} \dot{p} \\ \dot{\Theta} \end{bmatrix} = \begin{bmatrix} J_t(\Theta) & O_{(3 \times 3)} \\ O_{(3 \times 3)} & J_r(\Theta) \end{bmatrix} \begin{bmatrix} v \\ \omega \end{bmatrix} \quad (22)$$

where $O_{(3 \times 3)}$ is the 3×3 zero matrix, $v = [v_x \ v_y \ v_z]^T \in \mathbb{R}^3$, $\omega = [\omega_x \ \omega_y \ \omega_z]^T \in \mathbb{R}^3$ denote the translational velocity and the angular velocity of F_B relative to F_A respectively, both expressed in the Body-Fixed frame. The transformation matrices $J_t(\Theta)$, $J_r(\Theta) \in \mathbb{R}^{3 \times 3}$ are given by

$$J_t(\Theta) = \begin{bmatrix} c_\phi c_\psi & s_\phi s_\theta c_\psi - s_\psi c_\phi & s_\theta c_\phi c_\psi + s_\phi s_\psi \\ s_\psi c_\phi & s_\phi s_\theta s_\psi + c_\phi c_\psi & s_\theta s_\psi c_\phi - s_\phi c_\psi \\ -s_\theta & s_\phi c_\theta & c_\phi c_\theta \end{bmatrix} \quad (23)$$

$$J_r(\Theta) = \begin{bmatrix} 1 & s_\phi t_\theta & c_\phi t_\theta \\ 0 & c_\phi & -s_\phi \\ 0 & s_\phi / c_\theta & c_\phi / c_\theta \end{bmatrix} \quad (24)$$

The position of the end-effector with respect to F_A is $p_e = [x_e \ y_e \ z_e]^T = p + J_t(\Theta) r_e \in \mathbb{R}^3$. Its derivative is obtained as $\dot{p}_e = J_t(\Theta) v - J_t(\Theta) S(r_e) \omega$, using the formula $\dot{J}_t(\Theta) = J_t(\Theta) S(\omega)$ from [26]. The Body-Fixed and the End-Effector frame have the same orientation with reference to F_A , as mentioned in Section II, hence $\Theta_e = \Theta$. By combining the last results the following kinematic equation holds

$$\dot{\xi}_e = \begin{bmatrix} \dot{p}_e \\ \dot{\Theta} \end{bmatrix} = \underbrace{\begin{bmatrix} J_t(\Theta) & -J_t(\Theta) S(r_e) \\ O_{(3 \times 3)} & J_r(\Theta) \end{bmatrix}}_{J(\xi_e)} \begin{bmatrix} v \\ \omega \end{bmatrix} \quad (25)$$

where Θ_e is the orientation of F_E relative to F_A . The Jacobian matrix of the system $J(\xi_e) \in \mathbb{R}^{6 \times 6}$ relates in a straightforward way the linear velocity \dot{p}_e and the rate of change in the rotational angles $\dot{\Theta}$ of the end-effector expressed in F_A , with the Body-Fixed velocities v, ω .

B. Dynamic Model

The dynamic equations can be conveniently written with respect to the Body-Fixed frame by using the Newton-Euler formalism (the main concept is discussed extensively in [27], [28]), as

$$M \begin{bmatrix} \ddot{v} \\ \ddot{\omega} \end{bmatrix} + C(v) \begin{bmatrix} v \\ \omega \end{bmatrix} = \begin{bmatrix} F \\ T \end{bmatrix}_B \quad (26)$$

where

$$M = \begin{bmatrix} mI_3 & -mS(r_G) \\ mS(r_G) & I_B \end{bmatrix}, \quad M > 0, \quad \dot{M} = 0 \quad (27)$$

is the inertia matrix,

$$C = \begin{bmatrix} mS(\omega) & -mS(\omega)S(r_G) \\ mS(r_G)S(\omega) & -S(I_B\omega) \end{bmatrix}, \quad C = -C^T \quad (28)$$

is the Coriolis-centripetal matrix, I_3 is the 3×3 identity matrix, m is the total mass of the system, I_B is the inertia

tensor expressed in F_B and $\nu = [v^\tau \ \omega^\tau]^\tau \in \mathbb{R}^6$ is the vector of the Body-Fixed velocities. The inertia tensor can be written as $I_B = I_G - mS(r_G)S(r_G)$ where I_G is the inertia tensor relative to the body's centre of gravity. The vectors $F|_B, T|_B \in \mathbb{R}^3$ describe the forces and torques acting on the system expressed in the Body-Fixed frame and can be derived as

$$\begin{aligned} \begin{bmatrix} F \\ T \end{bmatrix}_B &= \begin{bmatrix} F \lambda - m g J_t^\tau(\Theta) e_3 \\ E \lambda + \mu F \lambda - m g S(r_G) J_t^\tau(\Theta) e_3 \end{bmatrix} \\ &= \underbrace{\begin{bmatrix} F \\ E \end{bmatrix} \lambda}_{\text{propulsion forces/torques}} + \underbrace{\begin{bmatrix} O_{(3 \times 6)} \\ \mu F \end{bmatrix} \lambda}_{\text{reaction torques}} - \underbrace{m g \begin{bmatrix} I_3 \\ S(r_G) \end{bmatrix} J_t^\tau(\Theta) e_3}_{\text{gravitational forces/torques}} \end{aligned} \quad (29)$$

where $e_3 = [0 \ 0 \ 1]^\tau$. Combining (26), (29) and solving with respect to $[\dot{v}^\tau \ \dot{\omega}^\tau]^\tau$ we get

$$\begin{aligned} \begin{bmatrix} \dot{v} \\ \dot{\omega} \end{bmatrix} &= -M^{-1}C(\nu) \begin{bmatrix} v \\ \omega \end{bmatrix} + M^{-1} \begin{bmatrix} F \\ E + \mu F \end{bmatrix} \lambda \\ &\quad - m g M^{-1} \begin{bmatrix} I_3 \\ S(r_G) \end{bmatrix} J_t^\tau(\Theta) e_3 \end{aligned} \quad (30)$$

$$\Leftrightarrow \dot{\nu} = \underbrace{H(\nu) + G(\xi_e)}_{B(\xi_e, \nu)} + N \lambda \quad (31)$$

where the matrices are defined as

$$H(\nu) = -M^{-1}C(\nu) \nu, N = M^{-1} \begin{bmatrix} F \\ E + \mu F \end{bmatrix} > 0 \quad (32)$$

$$G(\xi_e) = -m g M^{-1} \begin{bmatrix} I_3 \\ S(r_G) \end{bmatrix} J_t^\tau(\Theta) e_3 \quad (33)$$

$$B(\xi_e, \nu) = H(\nu) + G(\xi_e), B : \mathbb{R}^6 \times \mathbb{R}^6 \rightarrow \mathbb{R}^6 \quad (34)$$

IV. NONLINEAR CONTROL OF THE AERIAL MANIPULATOR

A manipulation task is usually given in terms of the desired position and orientation of the end-effector. The objective of this section is to design a controller for the aerial manipulator ensuring that the position $p_e(t)$ and the orientation $\Theta(t)$ of the end-effector track the desired Cartesian trajectory $\xi_{\text{des}}(t) = [p_{e,\text{des}}^\tau(t) \ \Theta_{\text{des}}^\tau(t)]^\tau \in \mathbb{R}^6$ asymptotically while all the closed loop signals remain bounded for all $t \geq 0$. Firstly, by using formulas (25), (31) the aerial manipulator model, including the kinematics and dynamics, can be written as

$$(S) : \begin{cases} \dot{\xi}_e = J(\xi_e) \nu \\ \dot{\nu} = B(\xi_e, \nu) + N \theta_\lambda^* \lambda + d(\xi_e, \nu, t) \end{cases} \quad (35)$$

where $d : \mathbb{R}^6 \times \mathbb{R}^6 \times \mathbb{R}_+ \rightarrow \mathbb{R}^6$ represents the unmodelled nonlinear dynamics and the environmental disturbances. The unknown matrix $\theta_\lambda^* = \text{diag}\{\theta_1^*, \dots, \theta_6^*\} \in \mathbb{R}^{6 \times 6}$ with $\theta_i^* \in [\theta_{\min}, \theta_{\max}] = [0.1, 1]$, is introduced to model the control actuation failures and the modeling errors among the thrusters of the system, e.g. if $\theta_i^* = 0.8$ then the i -th actuator has 20 % controller effectiveness reduction. The control inputs of the system are the six independent thrust forces $\lambda_i(t), i = 1, \dots, 6$ as mentioned in Section II. The

matrix N is full rank with low condition number which constitutes a vital result of the control oriented optimization from Section II.

The system (35) is highly nonlinear, cascaded and fully actuated in the well-known strict feedback form, with vector relative degree 2. For such systems, the backstepping controller design has proven to be successful [29], [30]. Due to the fact that the system is in the presence of the uncertainties θ_λ^* and the disturbances $d(\xi_e, \nu, t)$, a robust adaptive controller will be designed in order to tackle them. The aim is to study if the proposed system with the resulting geometry from the optimization problems $(P_1), (P_2)$, the system specifications from Table II and the aforementioned uncertainties/disturbances from (35), is capable to perform specific trajectory tasks efficiently. In order to design the controller of the system (35), the following assumptions are required:

Assumption 1: The states of the system ξ_e, ν are available for measurement $\forall t \geq 0$ for the following control development.

Assumption 2: The desired trajectories ξ_{des} are known and bounded derivatives ($\xi_{\text{des}} \in \mathcal{L}_\infty, \ddot{\xi}_{\text{des}} \in \mathcal{L}_\infty$).

Assumption 3: The disturbance $d(\xi_e, \nu, t) = [d_1(\xi_e, \nu, t) \ \dots \ d_6(\xi_e, \nu, t)]^\tau$ is unknown but bounded with $|d_i(\xi_e, \nu, t)| \leq \Delta_i$ where Δ_i are unknown positive constants for all $i = 1, \dots, 6$ and $t \geq 0$. **Assumption 4:** It is assumed for all $t \geq 0$ that $-\frac{\pi}{2} < \theta(t) < \frac{\pi}{2}$. This ensures that the Jacobian matrix is nonsingular since $\det(J(\xi_e)) = 1/c_\theta$. This assumption is likewise utilized in [26], [31].

• **Step 1:** To begin with the backstepping controller design, the position-orientation error of the end-effector is defined as $z_1 = \xi_e - \xi_{\text{des}} \in \mathbb{R}^6$. By differentiating it and using (25) we get

$$\dot{z}_1 = J(\xi_e) \nu - \dot{\xi}_{\text{des}} \quad (36)$$

We view ν as a control variable and we define a virtual control law $\nu_{\text{des}} \in \mathbb{R}^6$ for (36). The error signal representing the difference between the virtual and the actual controls is defined as $z_2 = \nu - \nu_{\text{des}} \in \mathbb{R}^6$. Thus, in terms of the new state variable, (36) can be rewritten as $\dot{z}_1 = J(\xi_e) z_2 + J(\xi_e) \nu_{\text{des}} - \dot{\xi}_{\text{des}}$. Consider now the positive definite and radially unbounded quadratic Lyapunov function $V_1(z_1) = \frac{1}{2} \|z_1\|^2 = \frac{1}{2} z_1^\tau z_1$. By differentiating it with respect to time yields

$$\dot{V}_1 = z_1^\tau \dot{z}_1 = z_1^\tau \left\{ J(\xi_e) \nu_{\text{des}} - \dot{\xi}_{\text{des}} \right\} + z_1^\tau J(\xi_e) z_2 \quad (37)$$

The stabilization of z_1 can be obtained by designing an appropriate virtual control law

$$\nu_{\text{des}} = J^{-1}(\xi_e) \left\{ \dot{\xi}_{\text{des}} - K_1 z_1 \right\} \quad (38)$$

where the matrix $K_1 \in \mathbb{R}^{6 \times 6}, K_1 = K_1^\tau > 0$ represents the first controller gain to be designed. Hence, the time derivative of V_1 becomes $\dot{V}_1 = -z_1^\tau K_1 z_1 + z_1^\tau J(\xi_e) z_2$. The first term of on the right-hand of this equation is negative and the second term will be canceled in the next step.

• **Step 2:** For the second step we define the matrices of the parameter estimation errors as $\tilde{\Delta} = [\tilde{\Delta}_1 \ \dots \ \tilde{\Delta}_6]^\tau = [(\hat{\Delta}_1 -$

$\Delta_1) \cdots (\hat{\Delta}_6 - \Delta_6)]^\tau$ and $\tilde{\theta}_\lambda = \text{diag}\{(\hat{\theta}_1 - \theta_1^*), \dots, (\hat{\theta}_6 - \theta_6^*)\}$ where $\hat{\Delta}_i, \hat{\theta}_i$ are the estimations of the unknown parameters Δ_i, θ_i^* respectively. The time derivative of the error z_2 is $\dot{z}_2 = B(\xi_e, \nu) + N \hat{\theta}_\lambda^\tau \lambda + d(\xi_e, \nu, t) - \dot{\nu}_{\text{des}}$. The Lyapunov function candidate in this step is chosen as

$$V_2(z_1, z_2, \tilde{\Delta}, \tilde{\theta}_\lambda) = V_1 + \frac{1}{2} z_2^\tau z_2 + \frac{1}{2} \tilde{\Delta}^\tau \Gamma_\Delta^{-1} \tilde{\Delta} + \frac{1}{2} \text{tr}(\tilde{\theta}_\lambda^\tau \Gamma_\theta^{-1} \tilde{\theta}_\lambda)$$

where $\Gamma_\theta = \Gamma_\theta^\tau > 0, \Gamma_\Delta = \Gamma_\Delta^\tau > 0$ are diagonal adaptation gain matrices and $\text{tr}(\cdot)$ denotes the matrix trace. The time derivative of $V_2(z_1, z_2, \tilde{\Delta}, \tilde{\theta}_\lambda)$ is obtained as

$$\begin{aligned} \dot{V}_2 = & -z_1^\tau K_1 z_1 + z_2^\tau \{J^\tau(\xi_e) z_1 + B(\xi_e, \nu) + N \hat{\theta}_\lambda^\tau \lambda - \dot{\nu}_{\text{des}}\} \\ & + z_2^\tau d(\xi_e, \nu, t) + \tilde{\Delta}^\tau \Gamma_\Delta^{-1} \dot{\tilde{\Delta}} + \text{tr}(\tilde{\theta}_\lambda^\tau \Gamma_\theta^{-1} \dot{\tilde{\theta}}_\lambda) \end{aligned} \quad (39)$$

Using the $-z_1^\tau K_1 z_1 \leq -\lambda_{\min}(K_1) \|z_1\|^2$, $z_2^\tau d(\xi_e, \nu, t) \leq z_2^\tau \text{sgn}(z_2) \Delta$ and adding and subtracting the terms $z_2^\tau N \hat{\theta}_\lambda^\tau \lambda$, $z_2^\tau \text{sgn}(z_2) \hat{\Delta}$ in (39) the following inequality holds

$$\begin{aligned} \dot{V}_2 \leq & -\lambda_{\min}(K_1) \|z_1\|^2 + z_2^\tau \{J^\tau(\xi_e) z_1 + B(\xi_e, \nu) - \dot{\nu}_{\text{des}} \\ & + \text{sgn}(z_2) \hat{\Delta} + N \hat{\theta}_\lambda^\tau \lambda\} - z_2^\tau N \tilde{\theta}_\lambda^\tau \lambda \\ & - z_2^\tau \text{sgn}(z_2) \tilde{\Delta} + \tilde{\Delta}^\tau \Gamma_\Delta^{-1} \dot{\tilde{\Delta}} + \text{tr}(\tilde{\theta}_\lambda^\tau \Gamma_\theta^{-1} \dot{\tilde{\theta}}_\lambda) \end{aligned} \quad (40)$$

where $\lambda_{\min}(K_1)$ denotes the minimum eigenvalue of matrix K_1 , $\text{sgn}(z_2) = \text{diag}\{\text{sgn}(z_{2,1}), \dots, \text{sgn}(z_{2,6})\}$ and $\text{sgn}(\cdot)$ denotes the sign function. Rearranging the terms and using the property $a^\tau b = \text{tr}(b a^\tau)$, $\forall a, b \in \mathbb{R}^n$ we get

$$\begin{aligned} \dot{V}_2 \leq & -\lambda_{\min}(K_1) \|z_1\|^2 + z_2^\tau \{J^\tau(\xi_e) z_1 + B(\xi_e, \nu) - \dot{\nu}_{\text{des}} \\ & + \text{sgn}(z_2) \hat{\Delta} + N \hat{\theta}_\lambda^\tau \lambda\} + \tilde{\Delta}^\tau \{\Gamma_\Delta^{-1} \dot{\tilde{\Delta}} - \text{sgn}(z_2) z_2\} \\ & + \text{tr}\{\tilde{\theta}_\lambda^\tau (\Gamma_\theta^{-1} \dot{\tilde{\theta}}_\lambda - N^\tau z_2 \lambda^\tau)\} \end{aligned} \quad (41)$$

Given the form of \dot{V}_2 from (41) the adaptive control law and the corresponding parameter estimation update laws for the nonlinear system (35) to be designed, are

$$\begin{aligned} \lambda(\xi_e, \nu, \hat{\Delta}, \hat{\theta}_\lambda) = & (\hat{\theta}_\lambda)^{-1} N^{-1} \{\dot{\nu}_{\text{des}} - B(\xi_e, \nu) - J^\tau(\xi_e) z_1 \\ & - \text{sgn}(z_2) \hat{\Delta} - K_2 z_2\} \end{aligned} \quad (42)$$

$$\dot{\hat{\Delta}} = \Gamma_\Delta \{\text{sgn}(z_2) z_2 - \sigma \hat{\Delta}\} \quad (43)$$

$$\dot{\hat{\theta}}_\lambda = \Gamma_\theta \text{Proj}(\hat{\theta}_\lambda, N^\tau z_2 \lambda^\tau) \quad (44)$$

where $K_2 = K_2^\tau > 0$ is the second controller gain matrix, σ is a strictly positive gain (σ -modification rule [32]) and the projection operator $\text{Proj}(\cdot, \cdot)$ is the same as the one in [33] with the parameter δ to be designed. By substituting (42), (43), (44) into (41) and using the property $\tilde{\Delta}^\tau \dot{\tilde{\Delta}} = \frac{1}{2} \|\dot{\tilde{\Delta}}\|^2 + \frac{1}{2} \|\hat{\Delta}\|^2 - \frac{1}{2} \|\Delta\|^2$ the following inequality holds

$$\begin{aligned} \dot{V}_2 \leq & -\lambda_{\min}(K_1) \|z_1\|^2 - \lambda_{\min}(K_2) \|z_2\|^2 + \\ & \underbrace{\text{tr}\left\{\tilde{\theta}_\lambda^\tau [\text{Proj}(\hat{\theta}_\lambda, y) - y]\right\}}_{\leq 0, y = N^\tau z_2 \lambda^\tau} - \frac{\sigma}{2} \|\tilde{\Delta}\|^2 - \frac{\sigma}{2} \|\hat{\Delta}\|^2 + \frac{\sigma}{2} \|\Delta\|^2 \\ & \leq -\frac{\sigma}{2} \|\tilde{\Delta}\|^2 + \frac{\sigma}{2} \|\Delta\|^2 \end{aligned}$$

The projection operator invoked from [33] contributes to the negative semi-negativeness of the Lyapunov function since

by definition $\text{tr}\left\{\tilde{\theta}_\lambda^\tau [\text{Proj}(\hat{\theta}_\lambda, y) - y]\right\} \leq 0, \forall y$. Moreover, it guarantees that if $\hat{\theta}_i(0) \in [\theta_{\min}, \theta_{\max}]$ is chosen, then $\hat{\theta}_i(t) \in [\theta_{\min} - \delta, \theta_{\max} + \delta], \forall i = 1, \dots, 6, \forall t \geq 0$ for suitable $\delta > 0$. The last result protects the term $(\hat{\theta}_\lambda)^{-1}$ in (42) from singularity. By defining $\bar{w} = \frac{\sigma}{2} \|\Delta\|^2 > 0$ we result in

$$\dot{V}_2 \leq -\lambda_{\min}(K_1) \|z_1\|^2 - \lambda_{\min}(K_2) \|z_2\|^2 - \frac{\sigma}{2} \|\tilde{\Delta}\|^2 + \bar{w}$$

from which it follows that both errors z_1, z_2 and the parameter estimation $\tilde{\Delta}$ are uniformly ultimately bounded with respect to the sets $\Omega_1 = \{z_1 \in \mathbb{R}^6 : \|z_1\| \leq \sqrt{\bar{w}/\lambda_{\min}(K_1)}\}$, $\Omega_2 = \{z_2 \in \mathbb{R}^6 : \|z_2\| \leq \sqrt{\bar{w}/\lambda_{\min}(K_2)}\}$ and $\Omega_\Delta = \{\tilde{\Delta} \in \mathbb{R}^6 : \|\tilde{\Delta}\| \leq \sqrt{2\bar{w}/\sigma}\}$. Invoking that z_1, z_2 are bounded and $\xi_{\text{des}}, \nu_{\text{des}} \in \mathcal{L}_\infty$ then $\xi_e, \nu \in \mathcal{L}_\infty$. Since $\tilde{\Delta}, \hat{\Delta}, \hat{\theta}_\lambda, \theta_\lambda^*, \dot{\nu}_{\text{des}}$ are bounded then $\hat{\Delta}, \hat{\theta}_\lambda, \lambda \in \mathcal{L}_\infty$. Based on the above, it is proven that all closed loop signals remain bounded.

One important issue associated with the controller design is the analytical form of the time derivative of ν_{des} , which can be obtained from (38) as $\dot{\nu}_{\text{des}} = J^{-1}(\xi_e) \{\ddot{\xi}_{\text{des}} - \dot{J}(\xi_e) \nu_{\text{des}} - K_1 \dot{z}_1\}$, and the time derivative of $J(\xi_e)$, which can be calculated by using the $\dot{J}_r(\Theta) = \frac{\partial J_r}{\partial \phi} \dot{\phi} + \frac{\partial J_r}{\partial \theta} \dot{\theta}$, $\dot{J}(\xi_e) = \begin{bmatrix} \dot{J}_t(\Theta) & -\dot{J}_t(\Theta) S(r_e) \\ O_{(3 \times 3)} & \dot{J}_r(\Theta) \end{bmatrix}$.

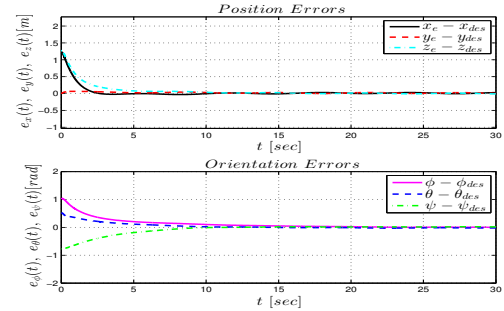


Fig. 4: Position and Orientation Errors

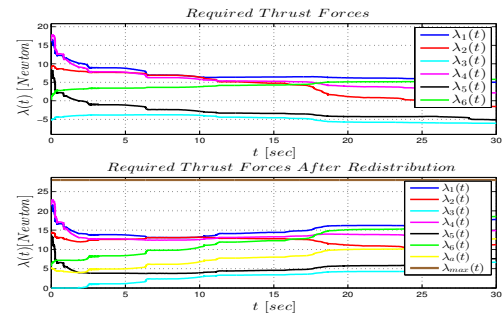


Fig. 5: Required Thrust Forces Using the Algorithm (17)

V. SIMULATION RESULTS

In this section, the results of a numerical simulation scenario are presented in order to demonstrate the performance of the proposed system. The dynamic model in (35) is utilized with system parameters which are depicted in Table II.

15 % controller effectiveness reduction is chosen with $\theta^* = 0.85 \text{ diag}\{1, 1, 1, 1, 1, 1\}$. The end-effector is forced to track the trajectory $p_{e,des}(t) = [\cos(0.5t) \sin(0.5t) 1.5 + 0.3t]^T$ with regulated orientation at $\Theta_{des} = [\frac{\pi}{3} \frac{\pi}{6} - \frac{\pi}{4}]^T$ with reference to the Earth-Fixed frame. The initial conditions of the system are set to $p_e(0) = r_e$, $p(0) = \Theta(0) = v(0) = \omega(0) = 0_{(3 \times 1)}$. The disturbance is set as $d(t) = [0.5 \ 0.4 \sin(2t) \ 0.4 \cos(t) \ 0.5 \ 0.5 \cos(0.8t) \ 0.6 \sin(t)]^T$ representing the unmodelled forces/torques and external disturbances. The initial values of the parameters estimations are set to $\hat{\theta}_1(0) = \dots = \hat{\theta}_6(0) = 0.7$ and $\hat{\Delta}_1(0) = \dots = \hat{\Delta}_6(0) = 0$. The controller gains are chosen as $K_1 = \text{diag}\{1, 1, 1, 0.3, 0.3, 0.3\}$, $K_2 = 8 \text{ diag}\{1, 1, 1, 1, 1, 1\}$. The adaptation gains are selected as $\sigma = 1.5$, $\Gamma_\Delta = 13 \text{ diag}\{1, 1, 1, 1, 1, 1\}$, $\Gamma_\theta = 0.1 \text{ diag}\{1, 1, 1, 1, 1, 1\}$. The parameter of the projection operator is set to $\delta = 0.05$. Fig. 4 shows the position and orientation tracking errors. The thrust forces are provided in Fig. 5. This paper is accompanied by a video demonstrating the simulation procedure of this Section. Due to space limitations, a video with an additional Scenario in better quality (HD) can be found at

<https://www.youtube.com/watch?v=DXnzu6XOrXs>

VI. CONCLUSIONS

Aerial robots physically interacting with the environment could be very useful for many applications. In this paper, we have presented the mechanical design of a novel aerial manipulator which was the result of technical optimization problems. A mathematical model for the kinematics and dynamics was derived in order to design an adaptive nonlinear controller to study the system while performing manipulation tasks. The simulation results illustrate the effectiveness of the proposed system and the controller to achieve tracking irrespectively of actuator failures, unmodelled dynamics and external disturbances. Future work mainly involves the construction of the aerial robot and the conduction of experimental trials for the proposed framework with the actual system, in order to verify the theoretical results of this paper.

REFERENCES

- [1] L. Marconi, R. Naldi, and L. Gentili, "Modelling and Control of a Flying Robot Interacting with the Environment," *Automatica*, vol. 47, no. 12, pp. 2571–2583, 2011.
- [2] A. Keemink, M. Fumagalli, S. Stramigioli, and R. Carloni, "Mechanical Design of a Manipulation System for Unmanned Aerial Vehicles," *IEEE International Conference on Robotics and Automation (ICRA)*, pp. 3147–3152, 2012.
- [3] A. Albers, S. Trautmann, T. Howard, T. Nguyen, M. Frietsch, and C. Sauter, "Semi-Autonomous Flying Robot for Physical Interaction with Environment," *IEEE Conference on Robotics Automation and Mechatronics (RAM)*, pp. 441–446, 2010.
- [4] P. Pounds, D. Bersak, and A. Dollar, "Grasping from the Air: Hovering Capture and Load Stability," *IEEE International Conference on Robotics and Automation (ICRA)*, pp. 2491–2498, 2011.
- [5] D. Mellinger, Q. Lindsey, M. Shomin, and V. Kumar, "Design, Modeling, Estimation and Control for Aerial Grasping and Manipulation," *IEEE/RSJ International Conference on Intelligent Robots and Systems (IROS)*, pp. 2668–2673, 2011.
- [6] V. Ghadiok, J. Goldin, and W. Ren, "Autonomous Indoor Aerial Gripping Using A Quadrotor," *IEEE/RSJ International Conference on Intelligent Robots and Systems (IROS)*, pp. 4645–4651, 2011.
- [7] D. Mellinger, M. Shomin, N. M. Nathan, and V. Kumar, "Cooperative Grasping and Transport Using Multiple Quadrotors," *Distributed Autonomous Robotic Systems*, vol. 83, pp. 545–558, 2013.
- [8] R. Ritz, W. Muller, M. Hehn, and R. D'Andrea, "Cooperative Quadcopter Ball Throwing and Catching," *IEEE/RSJ International Conference on Intelligent Robots and Systems (IROS)*, pp. 4972–4978, 2012.
- [9] G. Jiang and R. Voyles, "Hexrotor UAV Platform Enabling Dextrous Interaction with Structures-Flight Test," *2013 IEEE International Symposium on Safety, Security, and Rescue Robotics (SSRR)*, pp. 1–6, 2013.
- [10] F. Huber, K. Kondak, K. Krieger, D. Sommer, M. Schwarzbach, M. Laiacker, I. Kossyk, S. Parusel, S. Haddadin, and A. Albu-Schaffer, "First Analysis and Experiments in Aerial Manipulation Using Fully Actuated Redundant Robot Arm," *(IROS)*, 2013.
- [11] M. Kobilarov, "Nonlinear Trajectory Control of Multi-Body Aerial Manipulators," *Journal of Intelligent and Robotic Systems*, vol. 73, no. 1–4, pp. 679–692, 2014.
- [12] S. Kim, S. Choi, and H. Kim, "Aerial Manipulation Using a Quadrotor with a Two DOF Robotic Arm," *IEEE/RSJ International Conference on Intelligent Robots and Systems (IROS)*, pp. 4990–4995, 2013.
- [13] M. Orsag, C. Korpela, and P. Oh, "Modeling and Control of MM-UAV: Mobile Manipulating Unmanned Aerial Vehicle," *Journal of Intelligent and Robotic Systems*, vol. 69, no. 1–4, pp. 227–240, 2013.
- [14] A. Jimenez-Cano, J. Martin, G. Heredia, A. Ollero, and R. Cano, "Control of an Aerial Robot with Multi-Link Arm for Assembly Tasks," *(ICRA)*, pp. 4916–4921, 2013.
- [15] G. Padfield, "Helicopter Flight Dynamics, The Theory and Application of Flying Qualities and Simulation Modelling". AIAA education series, American Institute of Aeronautics and Astronautics, 1996.
- [16] L. N. Trefethen and D. Bau, "Numerical Linear Algebra". SIAM, 1997.
- [17] P. Gill, W. Murray, and M. Wright, "Numerical Linear Algebra and Optimization". Addison-Wesley Publishing Company, 1991.
- [18] K. Murty, "Linear Complementarity, Linear and Nonlinear Programming". Sigma Series in Applied Mathematics, Berlin: Heldermann Verlag, 1988.
- [19] M. Stein, "Large Sample Properties of Simulations Using Latin Hypercube Sampling," *Technometrics*, vol. 29, no. 2, pp. 143–151, 1987.
- [20] M. McKay, R. Beckman, and W. Conover, "A Comparison of Three Methods for Selecting Values of Input Variables in the Analysis of Output from a Computer Code," *Technometrics*, vol. 42, no. 1, pp. 55–61, 2000.
- [21] C. Audet and J. Dennis, "Analysis of Generalized Pattern Searches," *SIAM Journal on Optimization*, vol. 13, no. 3, pp. 889–903, 2003.
- [22] C. Audet and J. Dennis, "A Pattern Search Filter Method for Nonlinear Programming without Derivatives," *SIAM Journal on Optimization*, vol. 14, no. 4, pp. 980–1010, 2004.
- [23] V. Martinez, "Modelling of the Flight Dynamics of a Quadrotor Helicopter," Master Thesis, Cranfield University, 2007.
- [24] R. Prouty, "Helicopter Performance, Stability and Control". R.E. Krieger Publishing Company, 1995.
- [25] G. Antonelli, "Underwater Robots". Springer Tracts in Advanced Robotics, Springer International Publishing, 2013.
- [26] T. Madani and A. Benallegue, "Backstepping Control for a Quadrotor Helicopter," *IEEE/RSJ International Conference on Intelligent Robots and Systems (IROS)*, pp. 3255–3260, 2006.
- [27] T. Fossen, "Guidance and Control of Ocean Vehicles". John Wiley and Sons, 1994.
- [28] D. Bernstein, "Geometry, Kinematics, Statics and Dynamics". University of Michigan, 2013.
- [29] M. Krstić, I. Kanellakopoulos, and P. Kokotović, "Nonlinear and Adaptive Control Design". Wiley, 1995.
- [30] J. Zhou and C. Wen, "Adaptive Backstepping Control of Uncertain Systems: Nonsmooth Nonlinearities, Interactions Or Time-Variations". Springer, 2008.
- [31] M. Huang, B. Xian, C. Diao, K. Yang, and Y. Feng, "Adaptive Tracking Control of Underactuated Quadrotor Unmanned Aerial Vehicles via Backstepping," *American Control Conference (ACC)*, 2010.
- [32] E. Lavretsky and K. Wise, "Robust and Adaptive Control: with Aerospace Applications". Springer, 2012.
- [33] H. Khalil, "Adaptive Output Feedback Control of Nonlinear Systems Represented by Input-Output Models," *IEEE Transactions on Automatic Control*, vol. 41, pp. 177–188, Feb 1996.